A Unified Model for Injection-Locked Frequency Dividers

Shwetabh Verma, *Student Member, IEEE*, Hamid R. Rategh, and Thomas H. Lee, *Member, IEEE*

Abstract—Injection-locked frequency dividers (ILFDs) are versatile analog circuit blocks used, for example, within phase-locked loops (PLLs). An important attribute is substantially lower power consumption relative to their digital counterparts. The model described in this paper unifies the treatment of injection-locked and regenerative systems. It also provides useful design insights by clarifying the nature and role of the nonlinearity present in many mixer-based frequency conversion circuits. The utility of the model is demonstrated in the calculation of both the steady-state and dynamic properties of ILFD systems, and the subsequent computation of the corresponding phase noise spectrum. Illustrative circuit examples show close correspondence between theory and simulation. Finally, measurement results from a 5.4-GHz divide-by-2 ILFD fabricated in 0.24-μm CMOS show close correspondence between experiment and theory.

Index Terms—CMOS analog integrated circuits, frequency dividers, injection locking, locking range, loop bandwidth, oscillators, phase noise, phase-locked loops (PLLs).

I. INTRODUCTION

INJECTION-LOCKED frequency dividers (ILFDs) are analog circuit blocks that are useful in phase-locked loops (PLLs), among others, because they can consume much less power than conventional digital implementations. The ILFDs considered here fall under the broader class of regenerative frequency conversion circuits. Traditionally, a distinction has been drawn between injection-locked [1]–[3] and regenerative systems [4]–[6]. According to this tradition, injection-locked systems are free-running oscillators which lock in phase and frequency to an injected input signal, while regenerative systems do not free-run; they require an injected signal to produce an output. Previous theoretical treatments overlook the deep link between these two types of systems. It is also often difficult to extract circuit design insights from many models.

The model presented in this paper subsumes into a single treatment most circuits which accomplish frequency conversion by division. It identifies the role of the nonlinearity of most mixer-based frequency conversion circuits. This model is then used for calculating both the steady-state and dynamic properties of ILFD systems. The phase noise spectrum is computed using these results, and some illustrative circuit examples are provided at the end to provide experimental support for the theoretical predictions of the model. It is shown that within its locking range, the ILFD behaves much like a PLL. One important difference is that the loop bandwidth and the locking range
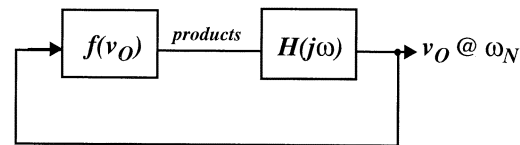
Fig. 1. General model for a free-running oscillator.

of the ILFD are controllable by the amplitude of the injected signal. Attention is paid throughout to the acquisition of design insight.

II. UNIFIED MODEL FOR THE INJECTION-LOCKED OSCILLATOR

In this section, we first discuss the case of a free-running oscillator, followed by an introduction to injection-locked oscillators. The attributes and weaknesses of some recently published models are considered before introducing a new unified model for injection-locked oscillators. As will be seen, a focus on system behavior in the weak injection regime provides important general insights into the operation of ILFDs.

Free-Running Oscillator

A general model for an oscillator is given in Fig. 1. It consists of a nonlinear gain block f and a linear filter $H(j\omega)$. The filter can be implemented any number of ways, such as with a cascaded RC [2] or LC network [3]. Let us assume that the oscillator operates at a natural oscillation frequency ω_N and that the filter $H(j\omega)$ suppresses frequencies far from ω_N. Let us call the steady-state output of the oscillator v_O.

Provided that f is a memoryless function, we can express it as a polynomial series of the form

$$f(v_O) = \sum_{m=0}^{\infty} a_m \cdot v_O^m \qquad (1)$$

where the coefficients a_m of the polynomial are constant. To analyze the steady-state solution of the free-running oscillator, we invoke the Barkhausen criterion [12], which states that the magnitude of the loop gain should be one, while the phase of the loop gain should be a multiple of 2π. Assume that v_O is sinusoidal of the form $v_O = V_O \cos(\omega_N t + \varphi)$. Harmonics of ω_N are generated as v_O is operated on by f. Substituting for v_O into (1) and expressing the result as a Fourier series, we obtain

$$\text{products} = f(V_O \cos(\omega_N t + \varphi))$$
$$= \sum_{m=0}^{\infty} C_m(V_O) \cdot \cos(m\omega_N t + m\varphi). \qquad (2)$$

The coefficients C_m depend on the nonlinearity f and are functions of the output amplitude V_O. Let the coefficient C_1 rep-
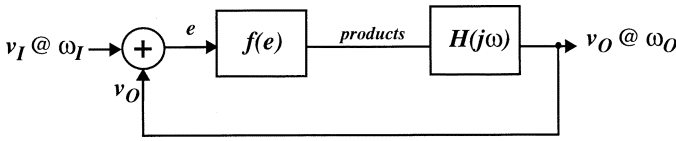
Fig. 2.   Common model for the injection-locked oscillator [3].

resent the gain of f at the frequency ω_N. Assuming the filter $H(j\omega)$ suppresses all frequency components other than those at ω_N, we can write the magnitude and phase conditions around the loop as follows:

$$|C_1| \cdot |H(j\omega_N)| = V_O \tag{3}$$

and

$$\angle C_1 + \angle H(j\omega_N) = 2k\pi \tag{4}$$

where k is an integer. Note that phase shift introduced by f can only be 0 or π, depending on the sign of C_1. The phase condition expressed in (4) states that the phase contributed by $H(j\omega)$ at ω_N must be zero (or π), modulo 2π. By contrast, we shall see later that the allowable phase shift contributed by the nonlinearity f in an injection-locked oscillator is a function of the injected signal.
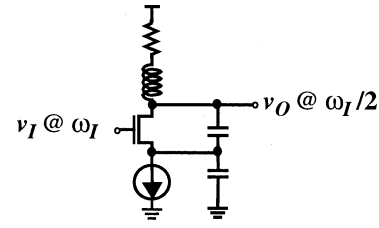
Injection-Locked Oscillator: Model 1 (Adler)

Injection-locked oscillators track the phase and frequency of an impressed signal. The output frequency ω_O of the oscillator may be the input frequency ω_I itself, or a submultiple or harmonic of ω_I. It may not necessarily be equal to ω_N, the oscillator's natural oscillation frequency in the absence of an injected signal. The mechanism of injection-locking for a small injected signal has been well described by Adler [1]. A simple, popular model which has been used to describe injection-locked oscillators is shown in Fig. 2 [3]. In this model, the two inputs v_I and v_O simply add before being operated on by the nonlinearity f. The nonlinearity is needed both for amplitude stability and to enable frequency mixing. This model gives particularly useful design insight when the model is a direct physical representation of the circuit. In such circuits, the input and output signals are summed and the result passes through a nonlinearity. The linear filter $H(j\omega)$ suppresses all frequencies far from ω_O, the frequency of oscillation.

We are interested in the frequency range over which the oscillator can track the injected signal. To compute this locking range, we again apply the Barkhausen criterion, just as in analyzing the free-running oscillator. As before, we can express f as a polynomial series, this time of the form
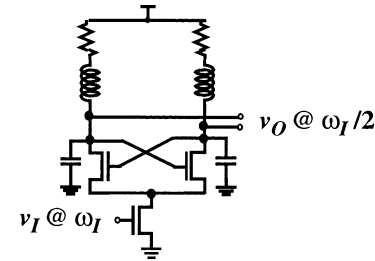
$$f(v_I + v_O) = \sum_{m=0}^{\infty} a_m \cdot (v_I + v_O)^m. \tag{5}$$

Let $v_O = V_O \cos(\omega_O t + \varphi)$ and $v_I = V_I \cos(\omega_I t)$. In this case, the products of f are given by [3]

$$\text{products} = f(v_I + v_O)$$
$$= \sum_{m=0}^{\infty} \sum_{n=0}^{\infty} K_{m,n} \cos(n\omega_I t) \cos(m\omega_O t + n\varphi). \tag{6}$$

(a)

(b)

Fig. 3.   Two injection-locked oscillator topologies.

If, for some integers m and n, $|m\omega_O \pm n\omega_I| = \omega_O$, then the corresponding output terms in (6) will exist at the frequency of oscillation ω_O. When these terms are combined, the output of f has a resulting phase shift with respect to the input signal. Unlike the free-running oscillator, the phase shift introduced by f is not restricted to 0 or π, and instead depends upon the strength of injection and the input frequency. To compensate for the extra phase shift due to the injection, the phase shift contributed by $H(j\omega)$ must change so that the net phase around the loop remains $2k\pi$. The loop changes the frequency of oscillation to accommodate the phase condition. This mechanism thus enables the oscillator frequency to track ω_I. When the input frequency ω_I is too large, $H(j\omega)$ cannot adjust and injection locking fails. A detailed derivation of the locking range based on this model has been provided in [3], and shows that failure to satisfy either the loop gain or loop phase condition can prevent locking.

As alluded to earlier, the model given in Fig. 2 is most useful for those circuits which have a one-to-one correspondence with it, that is, those in which the output and injected signals are actually summed in the circuit, and subsequently pass through the nonlinearity. One such circuit topology is shown in Fig. 3(a). However, in other cases, such as Fig. 3(b), the model becomes less physically meaningful. In fact, the latter circuit behaves much like a single-balanced mixer, in which v_I multiplies with v_O due to the action of the differential pair. In such cases, we should change the nature of the nonlinearity in our model so that we may get further design insight. We can then identify the important parameters upon which the performance of the ILFD depends and design an optimized circuit.

Injection-Locked Oscillator: Model 2 (Miller)

Miller [4] proposed regenerative frequency conversion circuits which, in the absence of an injected signal, do not oscillate. Nevertheless, we can model the injection-locked oscillator shown in Fig. 3(b) with a generalized Miller-type model [2], as
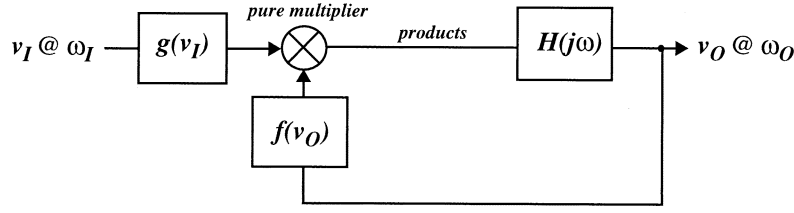
Fig. 4.   Miller-type model for the injection-locked oscillator [2].

shown in Fig. 4. Assume that the linear filter $H(j\omega)$ filters out all frequencies other than ω_O, the frequency of forced oscillation.

Note that we now have two memoryless nonlinear functions, f and g, which could represent nonlinearities inherent in practical approximations to pure multipliers, for example. The output of the mixer in the figure is of the form $f \cdot g$. Here, the function g could model the transconductor in a single-balanced Gilbert-type mixer, which produces an RF current riding on a dc current. In the absence of an RF current, the bias current will still allow the oscillator to free-run if there is sufficient loop gain. Since the transconductor may not be linear, harmonics of the injected signal may exist at the output of g, modeled as

$$g(v_I) = \sum_{n=0}^{\infty} b_n \cdot v_I^n. \tag{7}$$

If the function f models the differential pair in the Gilbert example, its action could be represented as

$$f(v_O) = \sum_{m=0}^{\infty} a_m \cdot v_O^m. \tag{8}$$

Now let $v_O = V_O \cos(\omega_O t + \varphi)$ and $v_I = V_I \cos(\omega_I t)$. The output of the mixer is then given by a product of Fourier series

$$\begin{aligned} \text{products} &= f \cdot g \\ &= \left[\sum_{n=0}^{\infty} B_n \cos(n\omega_I t) \right] \\ &\quad \cdot \left[\sum_{m=0}^{\infty} A_m \cos(m\omega_O t + m\varphi) \right]. \end{aligned} \tag{9}$$

In (9), the coefficients B_n are functions of the input amplitude V_I only, while A_m are functions of the output amplitude V_O. We can then determine which products lie at ω_O. The locking range calculation for such a general system will be very similar to that shown in [2]. While this model is quite general, and predicts the existence of sub- and superharmonic injection locking, it has its limitations. Specifically, the mixing of spectral components suggested by (9) might not be quite accurate, because the coefficients A_m and B_n could be functions of both V_O and V_I in practice.

Injection-Locked Oscillator: Model 3 (Unified)

To derive a more general model for the injection-locked oscillator, consider the block diagram shown in Fig. 5. Let us assume that f is a memoryless nonlinear function of both v_I and v_O. As before, the linear filter $H(j\omega)$ rejects frequency components far
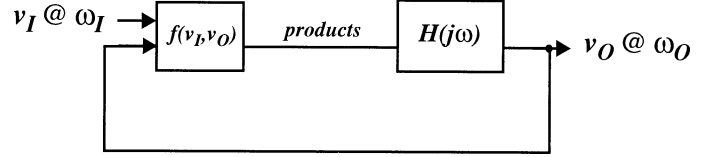

Fig. 5.   General model for the injection-locked oscillator.

from ω_O. For injection-locked oscillators, a convenient function representing f is

$$f(v_I, v_O) = \sum_{m=0}^{\infty} a_m(v_I) \cdot v_O^m. \tag{10}$$

Using a Taylor series expansion of v_I around a dc point V_{dc}, f can be written as

$$\begin{aligned} f(v_I, v_O) = \sum_{n=0}^{\infty} \frac{(v_I - V_{\text{dc}})^n}{n!} \\ \cdot \left[\sum_{m=0}^{\infty} \left. \frac{\partial^n}{\partial v_I^n} a_m(v_I) \right|_{v_I = V_{\text{dc}}} v_O^m \right]. \end{aligned} \tag{11}$$

The expression in (11) applies specifically to functions of the form (10). Let us assume that the magnitude of the injection is weak compared to the static bias point, i.e., v_I is close V_{dc}. In this case, we only consider terms with $n < 2$ in (11)

$$\begin{aligned} f(v_I, V_O) \cong \sum_{m=0}^{\infty} a_m(V_{\text{dc}}) \cdot v_O^m + (v_I - V_{\text{dc}}) \\ \cdot \left[\sum_{m=0}^{\infty} \tilde{a}_m(V_{\text{dc}}) \cdot v_O^m \right] \end{aligned} \tag{12}$$

where

$$\tilde{a}_m(V_{\text{dc}}) = \left. \frac{\partial}{\partial v_I} a_m(v_I) \right|_{v_I = V_{\text{dc}}}$$

is the derivative.

The first partial sum term in (12) is similar to (1) for the free-running oscillator. The second partial sum is due to the injection. For more accuracy, higher order terms can be added. The coefficients a_m and their derivatives can be determined either from the analytical form of f or extracted by measuring the effect of slight perturbations on the nonlinearity about the bias point V_{dc}. As we shall see in Sections V and VI, if the nonlinearity is memoryless, these coefficients give us all the information needed for a complete description of the behavior of an injection-locked oscillator about a bias point. If both v_I

and v_O are sinusoidal of the form $v_I = V_{dc} + V_I \cos(\omega_I t)$ and $v_O = V_O \cos(\omega_O t + \varphi)$, the full output of (11) can be written as

$$f(v_I, v_O) = \sum_{n=0}^{\infty} \frac{(V_I \cos(\omega_I t))^n}{n!}$$
$$\cdot \left[\sum_{m=0}^{\infty} \frac{\partial^n}{\partial v_I^n} a_m \Big|_{v_I = V_{dc}} (V_O \cos(\omega_O t + \varphi))^m \right]. \quad (13)$$

By taking advantage of the associativity of addition, we can re-group terms to express the bracketed quantity in (13) as a sum of harmonics of ω_O

$$f(v_I, v_O) = \sum_{n=0}^{\infty} \frac{(V_I \cos(\omega_I t))^n}{n!}$$
$$\cdot \left[\sum_{m=0}^{\infty} \frac{\partial^n}{\partial v_I^n} A_m \Big|_{v_I = V_{dc}} \cos(m\omega_O t + m\varphi) \right]. \quad (14)$$

In (14), the coefficients A_m have been introduced. Each A_m can be a function of all the a_m and V_O. Assuming weak injection as in (12) and simplifying ($n < 2$)

$$f(v_I, v_O) = \sum_{m=0}^{\infty} A_m \cos(m\omega_O t + m\varphi)$$
$$+ \frac{1}{2} \sum_{m=0}^{\infty} V_I \tilde{A}_m \cos[(m\omega_O \pm \omega_I)t + m\varphi] \quad (15)$$

where

$$\tilde{A}_m = \frac{\partial A_m}{\partial v_I} \Big|_{v_I = V_{dc}}.$$

In (15), we have an expression for the waveform at the output of f. The coefficients A_m are functions of a_m and V_O, while their derivatives $\tilde{A}_m$ are functions of $\tilde{a}_m$ and V_O. Note that si-nusoidal signals with coefficients A_m are generated by passing a solitary sinusoidal signal through the nonlinearity $f(v_I, v_O)$, while sinusoidal signals with coefficients $\tilde{A}_m$ are generated by passing the same sinusoidal signal through the *derivative* of the same nonlinearity with respect to v_I. Note that the first term of (15) is similar to (1) for the free-running oscillator, while the second term shows the mixer products due to the presence of the injected signal. Notice if the first sum term in (15) is small, then there may not be sufficient loop gain for oscillation in the ab-sence of an injected signal ($v_I = V_{dc}$). This case corresponds to that of traditional regenerative dividers. If there is a sufficiently large gain around the loop, the oscillator can free-run even in the absence of an injected signal. The system is then what is tra-ditionally referred to as an injection-locked oscillator.

Using (15), we may derive the steady-state conditions neces-sary for oscillation. We restrict ourselves to the case of super-harmonic locking, which is important for the study of frequency dividers. Assuming that $\omega_I = M\omega_O$ (where M is a positive integer), we can compute the products of (15) which exist at ω_O. Let us use the Barkhausen criterion to write the steady-state magnitude and phase expressions at the frequency ω_O

$$\sqrt{1 + k_0^2 + k_1^2 + 2(k_0 + k_1) \cos(M\varphi) + 2k_0 k_1 \cos(2M\varphi)}$$
$$\cdot |H(j\omega_O)| = \frac{V_O}{|A_1|} \quad (16)$$

$$\text{atan} \left[\frac{(k_1 - k_0) \sin(M\phi)}{1 + (k_1 + k_0) \cos(M\phi)} \right] + \angle H(j\omega_O) = 2k\pi \quad (17)$$

where

$$k_0 = \frac{V_I \tilde{A}_{M-1}}{2A_1} \quad \text{and} \quad k_1 = \frac{V_I \tilde{A}_{M+1}}{2A_1}.$$

Both of these important relationships need to be satisfied to sup-port locking. To find the full locking range of an ILFD, we find the frequency of the injected signal where either (16) or (17) fails. To derive a simplified analytical expression for the locking range, let us suppose that there is sufficient gain around the loop such that (16) is always satisfied. In such cases, the locking range is *phase limited*, and is thus determined solely by (17). Let us also suppose that the amplitude of the oscillation V_O does not change much as ω_0 changes. Therefore, A_1 and $\tilde{A}_{M\pm1}$ re-main constant as well. In this special case, the locking range can be computed directly from (17). For small frequency deviations, the phase response of the filter can be linearized about the nat-ural frequency of oscillation ω_N as $\angle H(j\omega_0) \cong S(\omega_0 - \omega_N)$, where S is a constant with dimensions of time. Assuming that $|k_1 + k_0| < 1$, we can show that

$$|\omega_0 - \omega_N| \le \left| \frac{1}{S} \cdot \text{atan} \left(\frac{k_1 - k_0}{\sqrt{1 - (k_1 + k_0)^2}} \right) \right| \quad (18)$$

where k_0 and k_1 both depend on V_O and V_I. We call this impor-tant quantity the output-referred phase-limited locking range of the ILFD.

III. TRANSIENT RESPONSE OF THE ILFD

Aside from the steady-state locking range, it is also important to understand the dynamics of ILFDs. The transient phase be-havior of an ILFD reveals much about its phase-noise filtering properties. We may evaluate the dynamics by considering how quickly the output phase or frequency would change if we were to suddenly step the phase or frequency injected into an ILFD.

Let us suppose that $v_I = V_{dc} + V_I \cos(M\omega_O t + \alpha)$ and $v_O = V_O \cos(\omega_O t + \varphi)$ where we consider phase on both the input and output signals (α and φ, respectively). When the system is in steady state, we can refer all the phase to the input or the output. The output phase of the ILFD can be perturbed by two sources: the phase noise of the input signal and internal phase noise of the ILFD. Consider the following two observations.

1) In steady state, there is a fixed phase relationship between α and φ. If α were to remain fixed and φ were to deviate slightly from its steady-state value due to internal noise, it would eventually return back to its steady-state value.

2) If α were to step suddenly to a different value, then φ would eventually stabilize to a new steady-state value in the absence of noise.
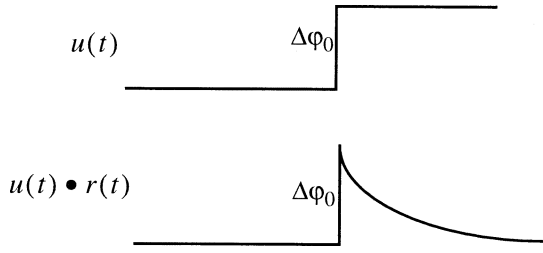
Fig. 6.   Phase response to an injected impulse of current.

As shown in the Appendix, the transient response of the ILFD is exponential for a weak injected signal and small frequency or phase perturbations. If ω_O is close to the ILFDs natural frequency of oscillation ω_N, the system has a first-order response with the following time constant:

$$\tau \cong \frac{1}{M} \left| \frac{S}{k_1 - k_0} \right|. \tag{19}$$

The same parameters that increase the phase-limited locking range (18) also reduce the time constant (19) of the system. In fact, an interesting result for all ILFDs is

$$|\omega_O - \omega_N|_{\text{max, phase-limited}} \cong 1/(M\tau). \tag{20}$$

That is, the phase-limited locking range of an ILFD is approximately $1/M$ times the 3-dB bandwidth of the first-order system response. This intuitively appealing result says that increasing the frequency locking range also speeds up the divider's transient performance.

IV. NOISE CONSIDERATIONS

We now use the results of the previous section to derive the phase-noise spectrum of the ILFD. We first consider the spectrum of a free-running oscillator, and then derive the spectrum of oscillator when it is injection locked.

According to the Hajimiri phase-noise model for free-running oscillators [7], the current-to-phase impulse response is given by

$$h_\varphi(t, \tau) = \frac{\Gamma(\omega_0 \tau)}{q_{\text{max}}} \cdot u(t - \tau) \tag{21}$$

where $\Gamma(\omega_0 \tau)$ is the impulse sensitivity function (ISF) which captures the true time variance of the system, q_{max} is a constant of proportionality, and $u(t - \tau)$ represents a time-shifted step function [7]. In a free-running oscillator, the phase cannot recover if it is perturbed because there is no reference which defines the "correct" phase. However, for injection-locked systems, phase will always recover in lock (Fig. 6), because a fixed phase relationship exists between the injected signal and the ILFD output at any given frequency of operation.

We can compute the phase response of the ILFD starting from (21), replacing the step function $u(t)$ with a decaying function $u(t) \bullet r(t)$, where $\bullet$ indicates convolution and $r(t)$ represents the impulse response of a high-pass filtering function. Assume that the ISF of the ILFD does not change substantially due to the presence of an injected signal. This assumption will hold generally if the injection is weak. So (21) then becomes

$$\tilde{h}_\varphi(t, \tau) = \frac{\Gamma(\omega_0 \tau)}{q_{\text{max}}} \cdot u(t - \tau) \bullet r(t). \tag{22}$$

Therefore, the expression for the output phase can be written as

$$\varphi = \int_{-\infty}^{\infty} \tilde{h}_\varphi(t, \tau) i(\tau) \, d\tau$$

$$= \int_{-\infty}^{\infty} \frac{\Gamma(\omega_0 \tau)}{q_{\text{max}}} \cdot (u(t - \tau) \bullet r(t)) i(\tau) \, d\tau. \tag{23}$$

Here, $i(\tau)$ represents the input noise current at time τ. Due to the linearity of convolution, the phase $\varphi(t)$ can be expressed as

$$\varphi(t) = \left(\int_{-\infty}^{\infty} \frac{\Gamma(\omega_0 \tau)}{q_{\text{max}}} \cdot u(t - \tau) i(\tau) \, d\tau \right) \bullet r(t). \tag{24}$$

Therefore, the phase of a locked system behaves just as the phase of a free-running system would behave, after passing through a linear time-invariant system with the impulse response $r(t)$. The power spectral densities (PSDs) are, therefore, related in the following manner:

$$L_{\varphi 1, \text{locked}}(\Delta\omega) = L_{\varphi, \text{free}}(\Delta\omega) \cdot |R(j\Delta\omega)|^2 \tag{25}$$

where $R(j\Delta\omega)$ is the Fourier transform of $r(t)$. Equation (25) shows that determination of the free-running phase noise of the ILFD permits calculation of the phase noise of the locked ILFD. To complete this computation, we must know $r(t)$. For small perturbations, we know that the transient response of the system is a decaying exponential, with a time constant τ given by (19). For a unit step response, the recovery waveform will be given by

$$\varphi(t) = u(t)^* r(t) = e^{-t/\tau}. \tag{26}$$

Defining $\omega_p = 1/\tau$, $R(s)$ can be calculated using the Laplace transform

$$\Phi_1(s) = \frac{1}{s} \cdot R(s) = \frac{1}{s + \omega_p}, \qquad R(s) = \frac{s}{s + \omega_p}. \tag{27}$$

Using $s = j\Delta\omega$ in (27) and substituting into (25), we can compute the PSD due to internal noise of the divider in the locked state

$$L_{\varphi 1, \text{locked}}(\Delta\omega) = L_{\varphi, \text{free}}(\Delta\omega) \cdot \frac{\Delta\omega^2}{\Delta\omega^2 + \omega_p^2}. \tag{28}$$

Note that to this point, we have implicitly assumed no phase noise from the input injection source, and considered only internal noise. We now neglect the internal phase noise and consider only the phase noise from the input. We know that the output phase of the divider tracks any small step changes in input phase scaled by the divide ratio $1/M$ (see the Appendix). The response of the system is, thus, a decaying exponential, as shown:

$$\Delta\varphi(t) = \frac{\Delta\alpha_0}{M} \left(1 - e^{-t/\tau} \right). \tag{29}$$

Therefore, if α were a time-varying signal with the Laplace transform $A(s)$, the output phase of the divider in the frequency domain will be

$$\Phi_2(s) = A(s) \cdot \left(\frac{\omega_p/M}{s + \omega_p} \right). \tag{30}$$

Therefore, if the injected signal is a noise process with PSD $L_{\alpha, ext}(\Delta\omega)$, the output phase noise has the PSD

$$L_{\varphi 2, \text{locked}}(\Delta\omega) = L_{\alpha, \text{ext}}(\Delta\omega) \cdot \frac{(\omega_p/M)^2}{\Delta\omega^2 + \omega_p^2}. \tag{31}$$
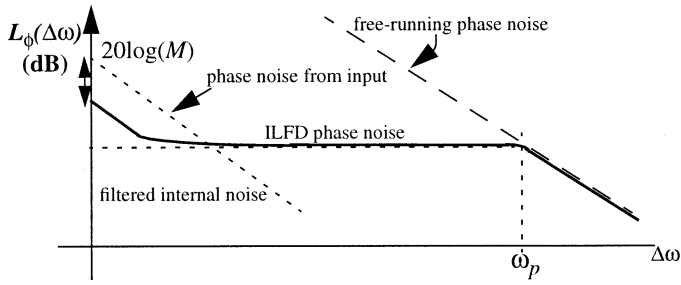
Fig. 7. Phase-noise spectrum of an ILFD.

Fig. 8. Schematic of the differential LC-based ILFD.

Since the two contributions to phase noise are generally independent, they are uncorrelated, and we can express the total phase noise as resulting from a superposition of individual noise powers

$$L_{\phi,\,\text{total}}(\Delta\omega) = L_{\phi,\,\text{free}}(\Delta\omega) \cdot \frac{\Delta\omega^2}{\Delta\omega^2 + \omega_p^2}$$
$$+ L_{\alpha,\,\text{ext}}(\Delta\omega) \cdot \frac{(\omega_p/M)^2}{\Delta\omega^2 + \omega_p^2}. \quad (32)$$

Notice that, just as in a first-order PLL, the internal free-running phase noise of the ILFD is filtered with a high-pass filter, while the noise from the external source is filtered with a low-pass filter. The extent of the filtering depends on the pole frequency ω_p. Also, wherever the internal phase noise is negligible, the phase noise of the output is dominated by the phase noise from the input, which the output tracks with a scale factor $1/M^2$. At $\Delta\omega$ far from ω_p, the phase noise of the locked oscillator approaches its free-running phase noise. Assuming that the internal free-running phase noise of the oscillator is of the form given in (33) [7]

$$L_{\phi,\,\text{prev}}(\Delta\omega) = \frac{\Gamma_{\text{rms}}^2}{q_{\text{max}}^2} \cdot \frac{\overline{i_n^2}/\Delta f}{2 \cdot \Delta\omega^2} \quad (33)$$

we can qualitatively see that the phase noise due to (32) will appear as shown in Fig. 7.

It should be clear that the frequency ω_p is analogous to the loop-bandwidth frequency of conventional PLLs. One important difference is that this loop bandwidth can be controlled by the strength of the injected signal. Therefore, we can get large loop bandwidths and fast locking times for strong signals, and low bandwidths with good source phase noise suppression with weak signals.

V. EXAMPLE 1: DIVIDE-BY-TWO LC ILFD

To illustrate further the utility of the unified model, we now use it to optimize the locking range of an LC oscillator operating as a divide-by-two ILFD. The locking range calculated from this section is compared against measurements in Section VII.

Consider the circuit shown in Fig. 8, which is a familiar differential ILFD topology [3]. Assume that the ILFD is locked and oscillating at the output frequency ω_O. An input voltage signal of frequency $\omega_I = 2\omega_O$ is injected into the tail device M3, producing a drain current which consists of a dc and an RF component. There is typically some capacitance at the tail
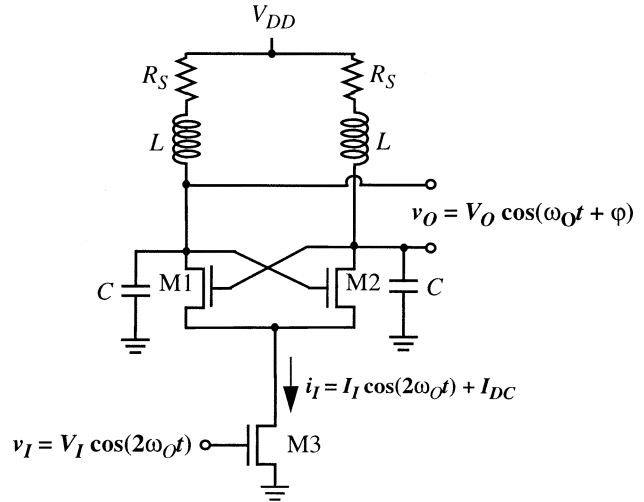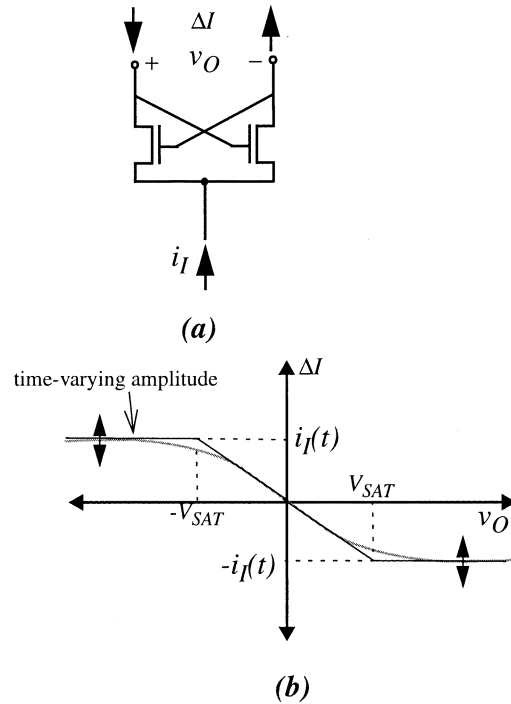

Fig. 9. Identifying the nonlinearity $f(i_I, v_O)$.

node, leading to parasitic current loss which increases with frequency. If the tail transconductor behaves nonlinearly, RF current at higher harmonics would tend to get filtered by this parasitic capacitance. Let us assume that otherwise, this capacitor does not greatly affect the transient behavior of the circuit.

Let the nonlinearity f of Fig. 5 be that of the cross-coupled pair formed by M1 and M2, as shown in Fig. 9(a). This non-linearity has two inputs, i_I and v_O. The output is a differential current ΔI, which gets filtered and converted to a voltage by the LC tank. This voltage is then fed back to the v_O input of f. For a given instantaneous value of $i_I(t)$, the ideal transfer characteristic of the differential pair is shown in Fig. 9(b). As $i_I(t)$ changes, this characteristic would both scale and distort. The saturated current value would change with $i_I(t)$, and V_{SAT} would also change. To simplify our analysis, let us assume that
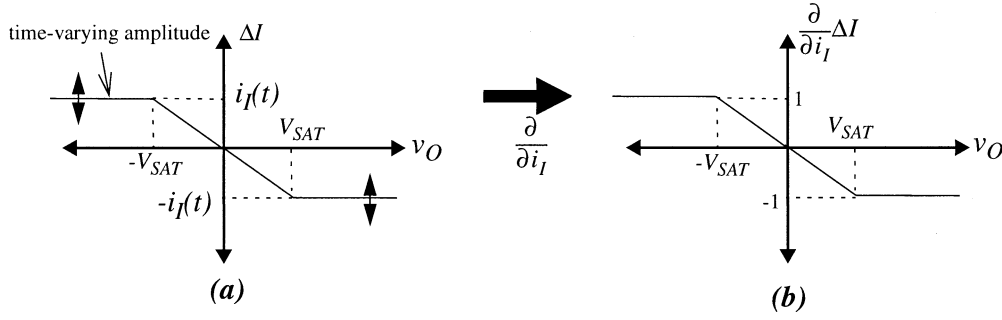
Fig. 10.   Nonlinearity $f(i_I, v_O)$ and its derivative with respect to i_I.
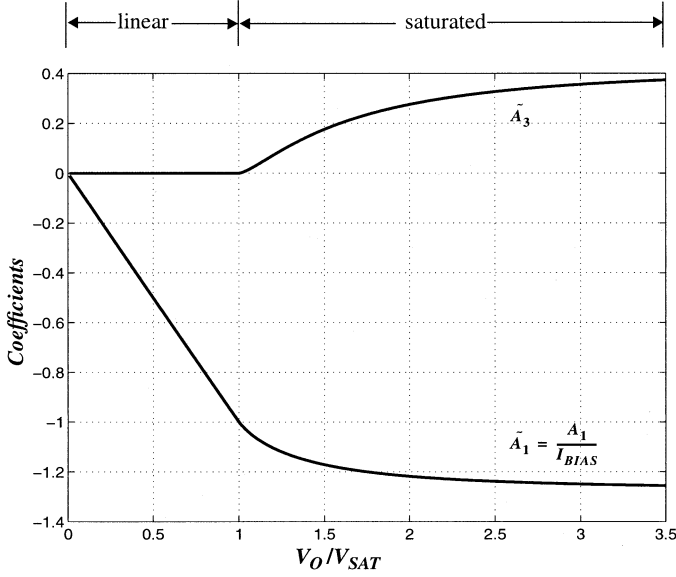

Fig. 11.   Normalized coefficients plotted versus V_O/V_{SAT}.

variation in $i_I(t)$ is small, so that we may neglect the minute variations of V_{SAT}. Therefore, we may approximate the characteristic of the cross-coupled pair by a piecewise linear function.

We now derive the steady-state solution for this divide-by-two ILFD. Using (12), we can linearize the response of the ILFD about $i_I = I_{\mathrm{dc}}$. Since we have neglected the variations in V_{SAT}, the nonlinearity and its derivative are related as shown in Fig. 10. In this case, it is easy to show that we have $A_m = I_{\mathrm{dc}} \cdot \tilde{A}_m$ in (15). For a divide-by-two circuit, we are interested in the coefficients A_1, $\tilde{A}_1$, and $\tilde{A}_3$ in (16) and (17). These coefficients have been calculated and are plotted as a function of V_O/V_{SAT} in Fig. 11.

The impedance formed by L, R_L, and C_{load} represents the filter $H(j\omega)$ in Fig. 8. This bandpass filter response can be linearized and expressed as [8]

$$H(j\omega) = \frac{H_0}{1 + j2Q \cdot \left(\frac{\omega - \omega_N}{\omega_N} \right)} \tag{34}$$

where H_0 represent the net parallel resistance across the tank at the resonant frequency ω_N. Note that the resonant frequency of the tank is also the natural oscillation frequency of the ILFD. Using impedance transformation, we can find that $H_0 = R_S(Q^2 + 1)$. Here, Q is the quality factor of the tank at resonance, approximately $\omega_N L/R_S$.
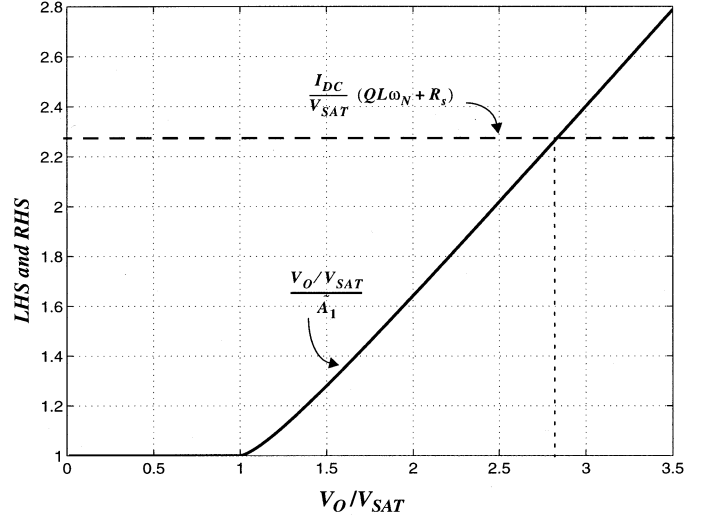
Fig. 12.   Solving for V_O.

Using the magnitude expression (16) and noting that $A_1 = I_{\mathrm{dc}} \cdot \tilde{A}_1$, we get

$$V_O = \left| \tilde{A}_1 \right| I_{\mathrm{dc}} R_s (Q^2 + 1)$$
$$\cdot \sqrt{1 + k_0^2 + k_1^2 + 2(k_0 + k_1)\cos(2\varphi) + 2k_0 k_1 \cos(4\varphi)} \tag{35}$$

where

$$k_0 = \frac{I_I}{2I_{\mathrm{dc}}} \quad \text{and} \quad k_1 = \frac{I_I}{2I_{\mathrm{dc}}} \cdot \frac{\tilde{A}_3}{\tilde{A}_1}.$$

To gain design insight, let us assume that both k_0 and k_1 are small compared with 1. In this case, the output amplitude of the oscillator remains relatively independent of the injection current i_I. We can approximate the output amplitude as

$$V_O \cong \tilde{A}_1 I_{\mathrm{dc}} R_s (Q^2 + 1)$$

or

$$\left[\frac{V_O/V_{\mathrm{SAT}}}{\tilde{A}_1} \right] \cong \frac{I_{\mathrm{dc}}}{V_{\mathrm{SAT}}} \cdot (QL\omega_N + R_s). \tag{36}$$

The right-hand side (RHS) and left-hand side (LHS) of (36) have been plotted as a function of V_O/V_{SAT} in Fig. 12. Note that the intercept of the two curves determines the final output amplitude. If the RHS is less than 1, no solution for V_O exists since there is insufficient loop gain for oscillation. From this plot, we see that to increase the final output amplitude of the ILFD, we
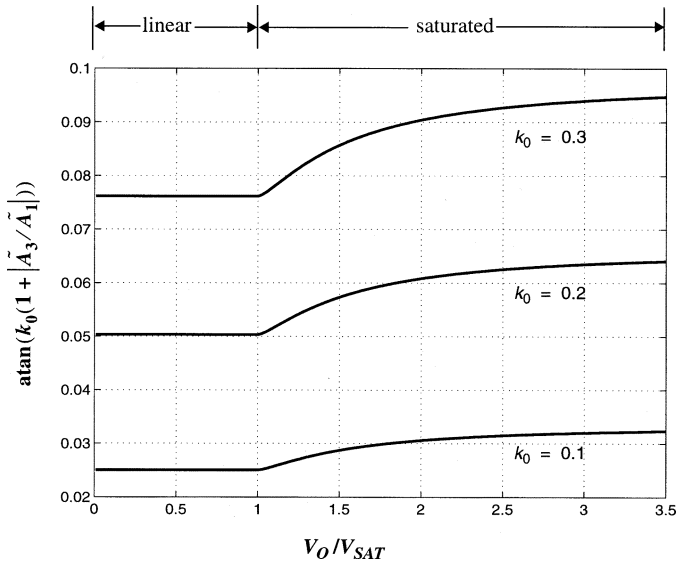
Fig. 13. Calculated normalized locking range as a function of V_O/V_{SAT} for $k_0 = 0.1, 0.2, 0.3$.

can increase the bias current, reduce the saturation voltage of the cross-coupled pair, or increase the QL product of the inductor at a given frequency. Note that reducing the V_{SAT} for the cross-coupled pair is equivalent to increasing its small-signal negative resistance.

From (18), the phase-limited locking range for weak injection current ($k_0 + k_1 \ll 1$) is approximately

$$|\omega_O - \omega_N| \leq \frac{\omega_N}{2Q} \cdot \mathrm{atan}\left(k_0\left(1 + \left|\tilde{A}_3/\tilde{A}_1\right|\right)\right). \quad (37)$$

In (37), we have used the fact that $\tilde{A}_3/\tilde{A}_1 < 0$ from Fig. 11, and have brought the absolute value sign within the argument of the arctangent. In Fig. 13, the relative locking range normalized by $2Q$ has been plotted as a function of V_O/V_{SAT} for k_0 equal to 0.1, 0.2, and 0.3. It is clear that the locking range increases by a maximum of approximately 33% as the output amplitude grows, for any injection strength.

Recall from (20) that the same parameters that maximize the phase-limited locking range of the ILFD also minimize the time constant and improve the phase-noise properties of the ILFD. To obtain a large locking range for the ILFD for a given bias current I_{dc} and injection amplitude I_I, we must keep a small Q for the LC tank while keeping a large output amplitude. While this may seem contradictory, observe that to keep the output amplitude large, we need to maximize the QL product. Note that $QL = \omega_N L^2/R_S$, so we may use large inductors constructed with thin metal lines. In this manner, we maintain a small Q while achieving a large QL product. Ultimately, the desired inductance will be limited by practical size of the resonating capacitor C or by the self-resonance frequency of the inductor itself. Therefore, it is in our interest to keep the "footprint" of the spiral inductor as small as possible. While we do not need a patterned ground shield [11] for this inductor design, since we want small Q and large self-resonance frequency, it does make the inductor performance more predictable. It is also important to note that injected current i_I is generated through the device M3, as shown in Fig. 8. Some of this current is lost in the capacitance in the drain node of M3 or the source-coupled node
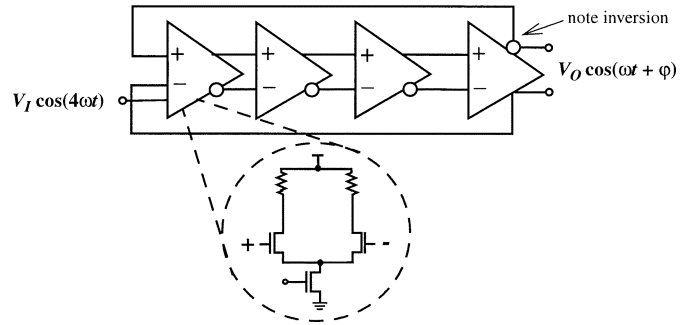

Fig. 14. Ring oscillator ILFD.

of M1 and M2. If the devices are large, or if the frequency of the injected signal is high, this loss may be significant. To alleviate this problem, we may tune out this capacitance using an inductor, as proposed by Wu [10].

## VI. EXAMPLE 2: DIVIDE-BY-FOUR RING OSCILLATOR ILFD

We next apply the new unified model to an injection-locked ring oscillator. We again calculate important steady-state as well as transient quantities. The theoretical results will be compared to HSPICE simulations.

Consider the circuit shown in Fig. 14. This circuit is a four-stage differential ring oscillator which also functions as a divide-by-four low-power frequency divider. This circuit topology is the same as presented in [2]. Each inverter is differential pair with a resistive load. All stages are identical, except that the input signal is injected into the tail current source of the first inverter as shown. Just as in the previous example, the input stage acts as a single-balanced mixer.

Some aspects of the analysis presented here are similar to that in [2]. However, we focus on the transient performance of the circuit, using a modeling approach similar to that used in the previous example. The nonlinearity f is the differential pair with inputs and outputs as shown in Fig. 9(a). Since this is a ring oscillator operating at lower frequencies, we can assume that its loop gain is large for small signals and that its output amplitude is large compared with the switching voltage of the differential pair for this circuit. In this case, we can assume that the differential pair switches abruptly. We can then use a simplified model of the nonlinearity f as shown in Fig. 15(a). For a weak injected current, the output of the nonlinearity f from (12) can be written as

$$f(i_I, v_O) = \sum_{m=0}^{\infty} a_m(I_{dc}) \cdot v_O^m$$
$$+ (i_I - I_{dc}) \cdot \left[\sum_{m=0}^{\infty} \tilde{a}_m(I_{dc}) \cdot v_O^m\right]. \quad (38)$$

Since the nonlinearity itself is approximated as a switching function in Fig. 15(a), the first term of (38) will yield a square wave with amplitude I_{dc} when a sinusoidal v_O is incident upon it about the static bias point $i_I = I_{dc}$. Furthermore, since the derivative of f with respect to i_I is also a switching function as seen from Fig. 15(b), the second term of (38) results in a mixing of the injected signal with another square wave
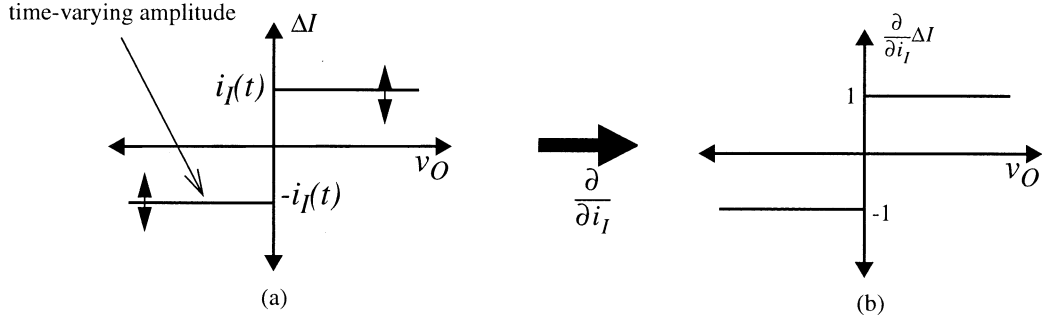
Fig. 15.   Nonlinearity $f(i_I, v_O)$ and its derivative.

with unit amplitude. Applying $i_I = I_{\rm dc} + I_I \cos(4\omega_O t)$ and $v_O = V_O \cos(\omega_O t + \varphi)$

$$f(i_I, v_O) = I_{\rm dc} \cdot \Pi(t) + I_I \cos(4\omega_O t) \cdot \Pi(t)$$
$$= [I_{\rm dc} + I_I \cos(4\omega_O t)] \cdot \Pi(t). \tag{39}$$

Expression (39) shows the output of an ideal single-balanced mixer. The mixing function $\Pi(t)$ is a square wave oscillating between -1 and 1, produced by the signal $v_O = V_O \cos(\omega_O t + \varphi)$ incident on the nonlinearity shown in Fig. 15(b). In this scenario, we have $A_m = I_{\rm dc} \cdot \tilde{A}_m$ for all the Fourier coefficients in (15). Therefore, the Fourier coefficients A_m are

$$A_m = \begin{cases} \dfrac{4I_{\rm dc}}{m\pi} \cdot (-1)^{(m-1)/2}, & \text{for } m = \text{odd} \\ 0, & \text{otherwise.} \end{cases} \tag{40}$$

The harmonic products generated by f are filtered and amplified by $H(j\omega)$, which models the low-pass filtering action of the four amplifier stages. This low-pass behavior results from the interaction of the output impedance of each buffer with the input capacitance of the following stage. We assume that the filter substantially suppresses the output products of the mixer at frequencies higher than ω_O. The low-pass filter $H(j\omega)$ can be modeled by

$$H(j\omega) = \frac{-H_O}{\left(1 + \dfrac{j\omega}{\omega_N}\right)^4}. \tag{41}$$

This approximation is valid as long as the number of stages is small. This is because, for a small number of stages, the ring freely runs at a frequency ω_N close to the dominant pole frequency of each stage. Therefore, the higher harmonics are well past this pole frequency. This output is fed back to the differential pair of the first inverter, thus closing the loop. Note that there is also one net inversion needed around the loop to allow the four-stage oscillator to free run. In (41), ω_N is the frequency of the free-running oscillator. Each stage contributes a phase shift of $\pi/4$, resulting in a total phase lag of 2π around the loop (including the inversion).

If there is sufficient gain around the loop, the output amplitude V_O is always large, even at the edge of the ILFD's locking range. In this case, the injection-locking dynamics are determined primarily by the phase relationship around the loop (phase limited) and, therefore, we can ignore the amplitude expression. A large amplitude is also required to excite the
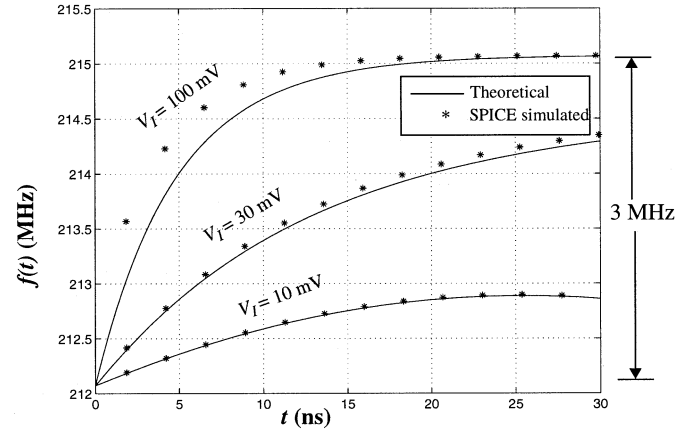
Fig. 16.   Transient frequency response to frequency perturbation of the ring ILFD for various V_I.
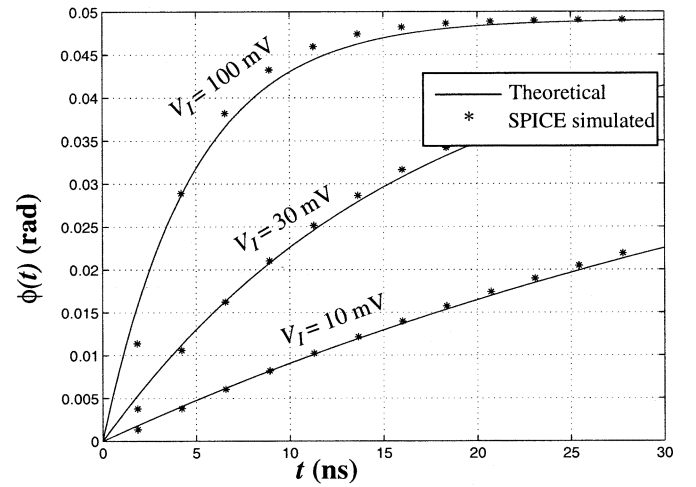
Fig. 17.   Transient phase response to phase perturbation of the ring ILFD for various V_I.

mixer's local oscillator (LO) port nonlinearity, which is the mechanism that makes possible division ratios greater than two.

Since we are assuming that the amplitude of the output is always large enough for the mixer to switch strongly, we need to consider only the phase-limited locking range. Assuming weak injection, we have

$$|\omega_O - \omega_N| \le \frac{\omega_N}{2} \cdot \text{atan}\left(\frac{4I_{\rm RF}}{15I_{\rm dc}}\right). \tag{42}$$
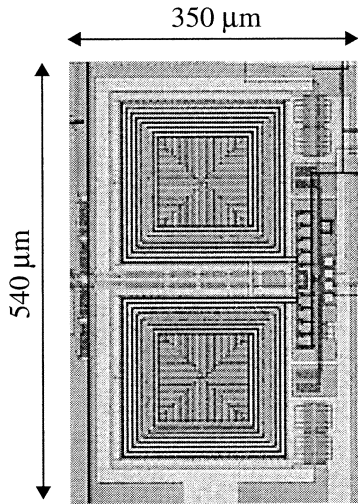
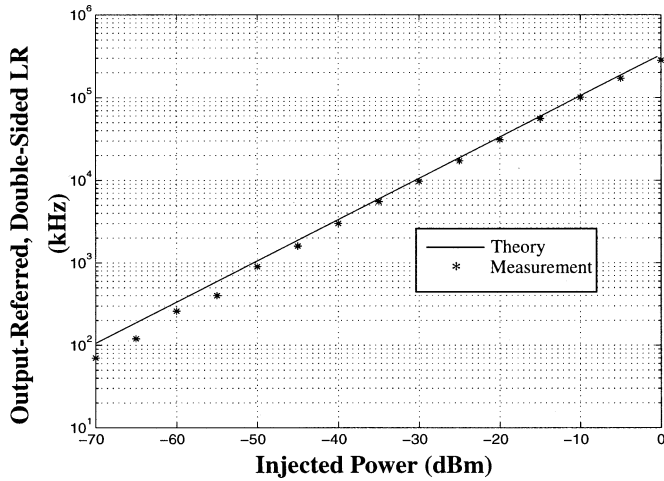Fig. 18. Die photo of the 5.4-GHz *LC* divide-by-two fabricated in 0.24-μm CMOS.

Fig. 19. Output-referred double-sided locking range as a function of input power.

Fig. 20. Phase noise spectrum of the ILFD for various injected powers.

Fig. 21. Output power as a function of injected power.

We can also calculate the characteristic time constant of this ILFD using (19) as

$$\tau \cong \frac{15 I_{\text{dc}}}{8 \omega_N I_{\text{RF}}}. \tag{43}$$

SPICE simulations of a 212-MHz divide-by-four ring oscillator ILFD are shown in Fig. 16. The device models used for simulation were for a 0.24-μm CMOS process. The transient output frequency response to a 12-MHz step change in injected frequency is shown for various injected voltage amplitudes. The discrete points show the cycle-to-cycle instantaneous frequency of the ILFD, computed at the zero crossings. The solid lines are the theoretically predicted curves, computed using (47), the more exact expression for the transient response. To numerically calculate the theoretical curves, we only need to know the amplitude and frequency of the injected signal, the bias current and transconductance of the nMOS into which it is injected, and the oscillation frequency ω_N. For $V_I = 100$ mV and $V_I = 30$ mV, the simulated frequency response looks exponential, and theoretical and simulated plots are similar. Since the input frequency
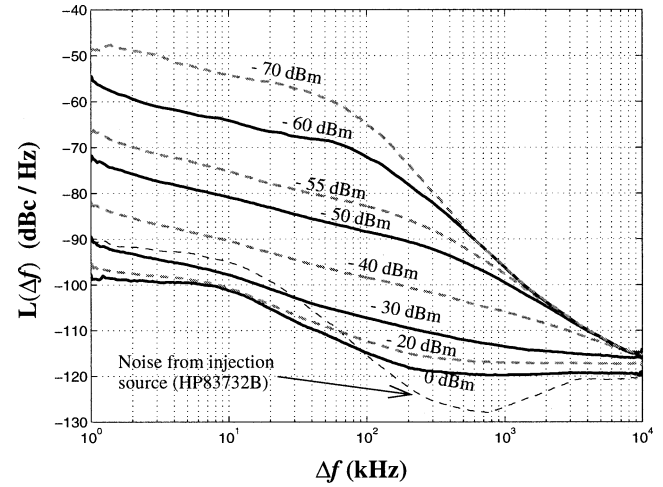
step is 12 MHz and the ILFD is a divide-by-four, both the theoretical and simulated curves converge to the same frequency step of 3 MHz. The small error is due to the pure switch approximation of the differential pair, and the small-signal injection assumption. In Fig. 16, it is interesting to note that for the weakest injected signal with $V_I = 10$ mV, the ILFD does not track the 12-MHz step in frequency. In this case, both simulation and theory [(47)] predict that the output "beats." This occurs when the phase condition cannot be satisfied and the oscillator cannot lock on to the injected signal. As a result, the output of the ILFD has signals with two different frequencies present. One is the ILFD's own oscillation frequency, and the other is from the injection source. Since these two frequencies are not the same, they heterodyne together to create output beats.

Fig. 17 shows the transient output phase response for an ILFD operating at ω_N for various injected amplitudes and for a step in input phase of $\pi/16$. The output phase changes exponentially and stabilizes at $\pi/64$. Once again, the discrete points show the cycle-to-cycle instantaneous phase of the ILFD, while the solid lines are the theoretical predicted curves, computed using (47). The two sets of curves correspond closely.
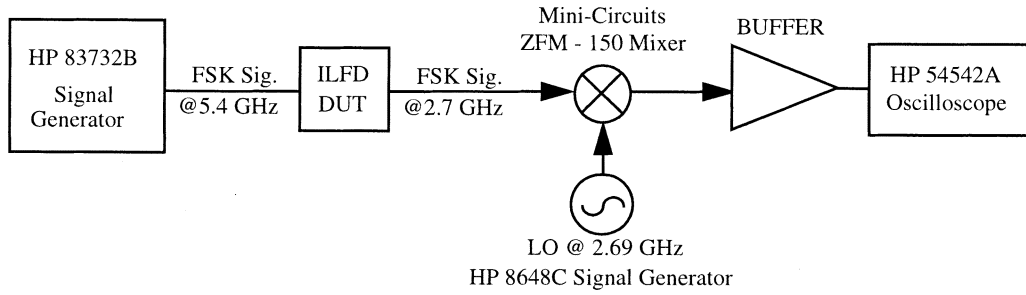
Fig. 22. Experimental setup to test the transient performance of the ILFD.

VII. MEASUREMENTS

Measurements were performed on a 5.4-GHz divide-by-two ILFD, shown in Fig. 18, which was fabricated in National Semiconductor's standard 0.24-μm CMOS process. The topology of the oscillator was the same as shown in Fig. 8. Fig. 19 shows the change in locking range as a function of the injected power. The 5.4-GHz injected signal was provided by an HP 83732B signal generator. The output spectrum of the ILFD at 2.7 GHz was observed using an HP 8563E spectrum analyzer. The measured input reflection coefficient S_{11} of the entire experimental setup (chip, package, and board) was better than -15 dB at around 5.4 GHz. A 50-Ω resistor was placed near the gate of the injection device (M3 in Fig. 8) on the chip. Care was taken to minimize all package and board parasitics. The theoretical (single-sided) locking range was calculated using (18), then multiplied by a factor of two to yield the double-sided locking range. The quality factor and inductance of the on-chip inductor were known. The characteristics of the differential pair were determined from simulations. It is clear that the measured locking range corresponds closely to the theoretical phase-limited locking range according to Fig. 19.

We know from (20) that the output-referred locking-range quantity is closely related to the dynamic behavior of the divider. Noting that M is 2, we observe that the output-referred double-sided locking range is approximately equal to $(2\pi\tau)^{-1}$ in hertz. The quantity τ is the characteristic time constant of the system defined in (19), and $1/\tau$ is identified in (32) as ω_P. Therefore, $\omega_P/2\pi$ should be approximately equal to the double-sided locking range in hertz.

Fig. 20 shows the measured output phase noise spectrum of the ILFD as a function of various injected powers. Note that all the curves eventually converge at high frequencies. This is theoretically predicted by (32). The presence of the injected signal tends to high-pass filter the free-running phase noise of the oscillator. The strength of the injected signal determines filter suppression and cutoff frequency ω_P. Comparing Figs. 19 and 20, note the similarity between $\omega_P/2\pi$ and locking range for corresponding injected power levels. For sufficiently large power levels, the free-running phase noise is greatly suppressed and the close-in phase noise of the divider settles to a value $20\log(M)$ below the phase noise of the reference source.

Recall that an important assumption underlying our phase-noise derivation is that the output oscillation amplitude of the divider does not change substantially in the presence of an input signal. Fig. 21 shows the change in output power as a function of injected power for this particular circuit. Note that it does not change greatly, implying that the unified model should provide valid predictions here.
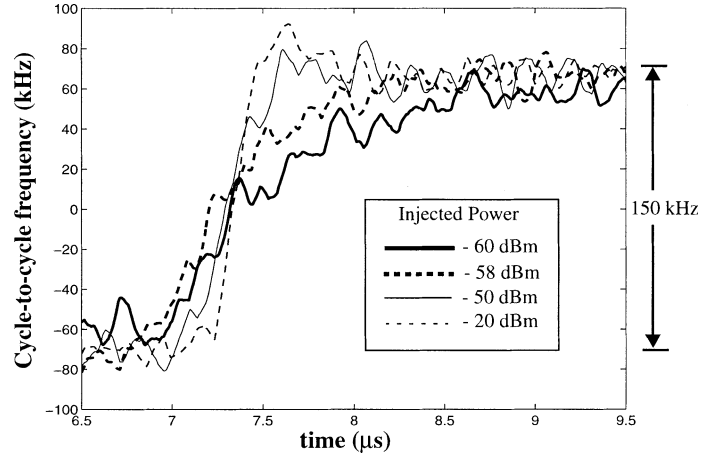

Fig. 23. Typical recovered FSK waveforms after noise averaging (mean adjusted to zero).

The dynamic frequency response of the ILFD was determined by injecting a frequency shift keying (FSK) signal, centered around 5.4 GHz, from a signal generator (HP 83732B). The sinusoidal output of the ILFD, centered around 2.7 GHz, was downconverted to 10 MHz with a commercially available mixer (Mini-Circuits ZFM-150) operating with a 2.69-GHz LO signal. The downconverted IF signal was fed into a data-capturing scope through a buffer, as shown in Fig. 22. From observing the cycle-to-cycle frequency count of the recovered sinusoidal signal, the frequency response of the divider was determined. This response was another FSK signal, modified by the properties of the divider. Due to substantial phase noise in the measurement setup, the recovered FSK signal was noisy. Therefore, a number of periods of the FSK signal had to be folded and averaged to reduce the noise.

Fig. 23 shows the rising edge of the recovered waveform for different injected powers. The mean frequency of waveform in the figure was shifted to zero for convenience. The peak-to-peak frequency variation of the reference signal was 300 kHz. As expected, the peak-to-peak variation of the output frequency of the ILFD was 150 kHz, which is within its locking range, even at -60-dBm injection. For relatively strong injection, the divider tracks the input signal closely. Note that the injected FSK waveform from the signal generator has a second-order (or higher) response, resulting in the peak and ripple-like behavior for the -20-dBm injected signal. However, as the injection strength is lowered, the response of the divider slows down, and the plot looks like an exponential. By taking the Fourier transform of such plots, and by treating the response for the -20-dBm injected signal as the clean reference, we can deconvolve the
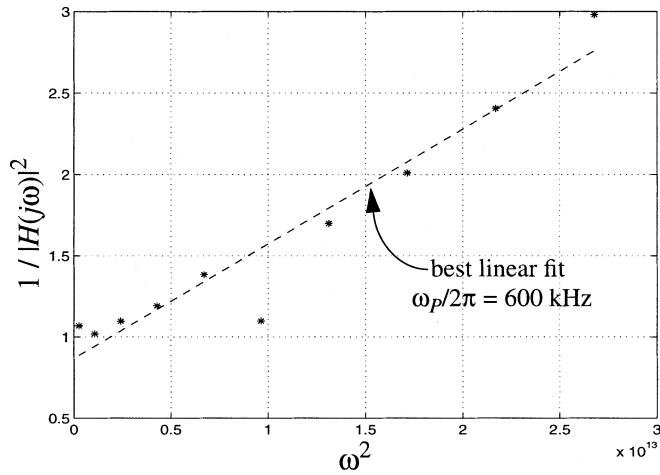
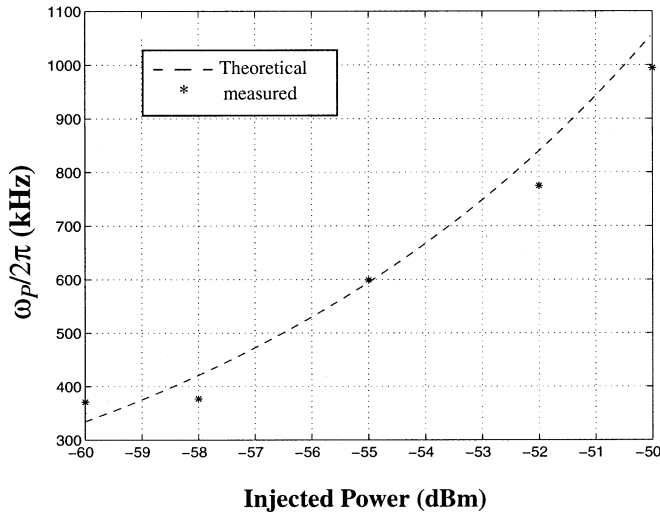Fig. 24.   Extracting ω_P for -55 dBm injected power.

Fig. 25.   Value of $\omega_P/2\pi$ extracted from measurements versus theory.

slow response $H(j\omega)$ of the divider for different injected power levels. We know that the response of a first-order low-pass filter with unity dc gain is of the following form:

$$H(j\omega) = 1 \Big/ \left(1 + \frac{j\omega}{\omega_P}\right). \quad (44)$$

Therefore

$$|1/H(j\omega)|^2 = 1 + \omega^2/\omega_P^2. \quad (45)$$

By plotting $|1/H(j\omega)|^2$ versus ω^2, computing the best least-squares linear fit, and calculating the slope, we can extract ω_P for each power level. An example plot for -55-dBm injected power is shown in Fig. 24. This procedure was carried out for several injected power levels. Fig. 25 shows the extracted and theoretical values of $\omega_P/2\pi$ plotted versus input power. Noting that $\omega_p = 1/\tau$, the theoretical ω_P was calculated using (19). Figs. 19 and 25 are expected to be nearly identical; they are, experimentally and theoretically, over the given input power range.

VIII. CONCLUSION

This paper presented a new model which allows the accurate determination of the steady-state, transient, and phase-noise

properties of a large class of practical injection-locked systems. The expressions yield greater design insight than do previously published models. The model has also been used to demonstrate that injection-locked systems and regenerative systems are essentially the same. The model also shows that within its locking range the ILFD has many PLL-like characteristics. It tracks the phase of the injected signal, acts as a low-pass filter for the phase noise from the source, and suppresses its own internal phase noise within its effective loop bandwidth. This loop bandwidth is closely related to the locking range of the ILFD. One important difference between ILFDs and PLLs is that the loop bandwidth of the ILFD is controllable by the amplitude of the injected signal. This is a useful result, since for the same ILFD, we can get a large loop bandwidth and fast locking times for strong signals, and low bandwidths with good source phase noise suppression with weak signals. Another major advantage is that ILFDs potentially consume much less power than entire PLLs, since they are just oscillators. When utilized as a prescalar in the feedback path of a PLL working as a frequency synthesizer, the ILFD can also potentially consume much less power than its digital counterpart, particularly at higher frequencies.

APPENDIX
DERIVATION OF THE CHARACTERISTIC TIME CONSTANT

Phase Step Response

Let the natural frequency of oscillation be ω_N. Assume that at $t = 0^-$, $v_I = V_{dc} + V_I \cos(M\omega_O t + \alpha_0)$ and $v_O = V_O \cos(\omega_O t + \varphi_0)$. Assume also that V_I is weak compared to V_{dc} and that V_O does not change significantly due to small phase or frequency perturbations. For small variations of frequency about ω_N (i.e., $\Delta\omega$), the phase response of $H(j\omega)$ can be linearized as $\angle H(j\omega) \cong S(\omega - \omega_N)$. The phase condition around the loop yields

$$\operatorname{atan}\left[\frac{(k_1 - k_0)\sin(M\varphi_0 - \alpha_0)}{1 + (k_1 + k_0)\cos(M\varphi_0 - \alpha_0)}\right] + S(\omega_O - \omega_N) = 2k\pi. \quad (46)$$

At $t = 0^+$, suppose that the input phase steps to a fixed value $\alpha_0 + \Delta\alpha_0$. The output phase gradually changes in response. Assume that the instantaneous phase at the output is $\varphi_0 + \Delta\varphi$. The instantaneous frequency at the output is $\omega_O + d\Delta\varphi/dt$. With the stated assumptions, the dynamic response of the system is entirely governed by the phase condition. The phase condition yields the general expression

$$\operatorname{atan}\left[\frac{(k_1 - k_0)\sin(M\varphi_0 - \alpha_0 + M\Delta\varphi - \Delta\alpha_0)}{1 + (k_1 + k_0)\cos(M\varphi_0 - \alpha_0 + M\Delta\varphi - \Delta\alpha_0)}\right]$$
$$+ S\left(\omega_O + \frac{d}{dt}\Delta\varphi - \omega_N\right) = 2k\pi. \quad (47)$$

Assuming that $M\Delta\varphi - \Delta\alpha_0$ is always small, and using (46), we get the following expression:

$$\frac{(k_1 - k_0)[k_1 + k_0 + \cos(M\varphi_0 - \alpha_0)]}{[(k_1 - k_0)\sin(M\varphi_0 - \alpha_0)]^2 + [1 + (k_1 + k_0)\cos(M\varphi_0 - \alpha_0)]^2}$$
$$\cdot (M\Delta\varphi - \Delta\alpha_0) + S\frac{d}{dt}\Delta\varphi \cong 0. \quad (48)$$

Equation (48) is a linear first-order differential equation whose time constant may appear complicated initially. If we assume that $\omega_O = \omega_N$, from (46) we get $M\varphi_0 - \alpha_0 = n\pi$, where n is any integer. Substituting into (48), we get

$$\pm \frac{1}{S} \frac{(k_1 - k_0)}{[1 \pm (k_1 + k_0)]} (M\Delta\varphi - \Delta\alpha_0) + \frac{d}{dt}\Delta\varphi \cong 0. \quad (49)$$

If $k_1 - k_0$ and S are both either positive or negative, then we get a stable solution for even n. If not, then an odd value of n gives us a stable solution. Notice that the time constant could be slightly different depending on the initial phase condition. However, if we assume that the injection is weak, then $k_1 + k_0 \ll 1$. If we consider only stable phase solutions, then notice that the phase of the solution recovers with approximately the time constant τ

$$\tau = \frac{1}{M} \left| \frac{S}{k_1 - k_0} \right|. \quad (50)$$

Note that the output phase recovers to $\varphi_0 + \Delta\alpha_0/M$ in steady state.

Frequency Step Response

Let us now consider what happens when we step the input frequency by a small amount. Expression (47) is still applicable here, with $\Delta\alpha_0$ now a linear ramp in phase. We can differentiate (47) with respect to time to find the output frequency response of the system. Rather than show the full analysis here, let us make some simplifications. Assume that the frequency step is not large compared to the ILFD's locking range, so that $M\Delta\varphi - \Delta\alpha_0$ always remains small. Let us also assume that $\omega_O = \omega_N$. In this case, we can take the derivative of (49) to find that the frequency time constant of the system is still approximately as given in (50).

Therefore, for small frequency and phase perturbations, the transient response of the system is first-order exponential with the time constant τ at the center of its locking range. We can now use this result to derive the phase-noise spectrum of the ILFD.

REFERENCES

[1] R. Adler, "A study of locking phenomena in oscillators," *Proc. IRE*, vol. 34, pp. 351–357, June 1946.
[2] R. J. Betancourt-Zamora, S. Verma, and T. H. Lee, "1-GHz and 2.8-GHz injection-locked ring oscillator prescalers," in *Symp. VLSI Circuits Dig. Tech. Papers*, June 2001, pp. 47–50.
[3] H. R. Rategh and T. H. Lee, "Superharmonic injection-locked frequency dividers," *IEEE J. Solid-State Circuits*, vol. 34, pp. 813–821, June 1999.
[4] R. L. Miller, "Fractional-frequency generators utilizing regenerative modulation," *Proc. IRE*, vol. 27, pp. 446–457, July 1939.
[5] A. S. Daryoush, T. Berceli, R. Saedi, P. Herczfeld, and A. Rosen, "Theory of subharmonic synchronization of nonlinear oscillators," in *IEEE MTTS Dig.*, vol. 2, 1989, pp. 735–738.
[6] R. G. Harrison, "Theory of regenerative frequency dividers using double-balanced mixers," in *IEEE MTT-S Dig.*, June 1989, pp. 459–462.
[7] A. Hajimiri, "Jitter and phase noise in electrical oscillators," Ph.D. dissertation, Stanford Univ., Stanford, CA, Nov. 1998.
[8] B. Razavi, "Analysis, modeling and simulation of phase noise in monolithic voltage-controlled oscillators," in *Proc. IEEE Custom Integrated Circuits Conf.*, May 1995, pp. 323–326.
[9] T. H. Lee, *The Design of CMOS Radio-Frequency Integrated Circuits*. Cambridge, U.K.: Cambridge Univ. Press, 1998.
[10] H. Wu and A. Hajimiri, "A 19-GHz 0.5-mW 0.35-μm CMOS frequency divider with shunt-peaking locking-range enhancement," in *IEEE Int. Solid-State Circuits Conf. Dig. Tech. Papers*, Jan. 2001, pp. 412–413, 471.
[11] P. Yue and S. Wong, "On-chip spiral inductors with patterned ground shields for Si-based RFICs," in *Symp. VLSI Circuits Dig. Tech. Papers*, June 1997, pp. 85–86.
[12] A. S. Sedra and K. C. Smith, *Microelectronic Circuits*. Oxford, U.K.: Oxford Univ. Press, 1991.

Shwetabh Verma (M'98) received the B.S. degree in electrical engineering from the University of Toronto, Toronto, ON, Canada, in 1998 and the M.S. degree in electrical engineering from Stanford University, Stanford, CA, in 2000. He is currently working toward the Ph.D. degree at Stanford University.

During the summer of 1999, he was with Sun Microsystems Laboratories, Mountain View, CA, where he designed and characterized integrated spiral inductors and transformers. His current research interests are in circuits and systems for low-cost wireless personal area networks (WPANs).

Mr. Verma was a recipient of the Stanford graduate fellowship in 1998.

Hamid R. Rategh was born in Shiraz, Iran, in 1972. He received the B.S. degree in electrical engineering from Sharif University of Technology, Tehran, Iran, in 1994, the M.S. degree in biomedical engineering from Case Western Reserve University, Cleveland, OH, in 1996, and the Ph.D. degree in electrical engineering from Stanford University, Stanford, CA, in 2001.

During the summer of 1997, he was with Rockwell Semiconductor System, Newport Beach, CA, where he was involved in the design of a CMOS dual-band GSM/DCS1800 direct conversion receiver. His current research interests are in low-power radio-frequency integrated circuits design for high data rate wireless systems.

Dr. Rategh was the recipient of the 1997 Stanford graduate fellowship. He was also a member of the Iranian team in the 21st International Physics Olympiad.

Thomas H. Lee (M'87) received the S.B., S.M., and Sc.D. degrees in electrical engineering from the Massachusetts Institute of Technology, Cambridge, in 1983, 1985, and 1990, respectively.

He joined Analog Devices, Norwood, MA, in 1990, where he was primarily engaged in the design of high-speed clock recovery devices. In 1992, he joined Rambus Inc., Mountain View, CA, where he developed high-speed analog circuitry for 500-Mbyte/s CMOS DRAMs. He has also contributed to the development of PLLs in the StrongARM, Alpha, and K6/K7 microprocessors. Since 1994, he has been a Professor of electrical engineering at Stanford University, Stanford, CA, where his research focus has been on gigahertz-speed wireline and wireless integrated circuits built in conventional silicon technologies, particularly CMOS. He is also a cofounder of Matrix Semiconductor, Santa Clara, CA. He authored *The Design of CMOS Radio-Frequency Integrated Circuits* (Cambridge, U.K.: Cambridge Univ. Press, 1998), and is a coauthor of three additional books on RF circuit design. He holds 23 U.S. patents.

Dr. Lee has twice received the Best Paper Award at the IEEE International Solid-State Circuits Conference (ISSCC). He was a coauthor of a Best Student Paper at ISSCC, was awarded the Best Paper prize at the IEEE Custom Integrated Circuits Conference, and is a Packard Foundation Fellowship recipient. He is an IEEE Distinguished Lecturer of the Solid-State Circuits and Microwave Societies. and